HAL
open science

Polarization constraints on the X-ray corona in Seyfert Galaxies: MCG-05-23-16

A. Marinucci, F. Muleri, M. Dovciak, S. Bianchi, F. Marin, G. Matt, F. Ursini, R. Middei, H. L. Marshall, L. Baldini, et al.

To cite this version:

A. Marinucci, F. Muleri, M. Dovciak, S. Bianchi, F. Marin, et al.. Polarization constraints on the X-ray corona in Seyfert Galaxies: MCG-05-23-16. Monthly Notices of the Royal Astronomical Society, 2022, 516 (4), pp.5907-5913. 10.1093/mnras/stac2634 . insu-03794870

HAL Id: insu-03794870

https://insu.hal.science/insu-03794870v1

Submitted on 6 Jul 2023

HAL is a multi-disciplinary open access archive for the deposit and dissemination of scientific research documents, whether they are published or not. The documents may come from teaching and research institutions in France or abroad, or from public or private research centers.

L'archive ouverte pluridisciplinaire **HAL**, est destinée au dépôt et à la diffusion de documents scientifiques de niveau recherche, publiés ou non, émanant des établissements d'enseignement et de recherche français ou étrangers, des laboratoires publics ou privés.

Monthly Notices of the ROYAL ASTRONOMICAL SOCIETY

MNRAS **516,** 5907–5913 (2022)
Advance Access publication 2022 September 29

https://doi.org/10.1093/mnras/stac2634

Polarization constraints on the X-ray corona in Seyfert Galaxies: MCG-05-23-16

A. Marinucci,[1★] F. Muleri,[2] M. Dovciak,[3] S. Bianchi,[4] F. Marin,[5] G. Matt,[4] F. Ursini,[4] R. Middei,[6,7] H. L. Marshall,[8] L. Baldini,[9,10] T. Barnouin,[5] N. Cavero Rodriguez,[11] A. De Rosa,[2] L. Di Gesu,[1] D. Harper,[11] A. Ingram,[12] V. Karas,[3] H. Krawczynski,[11] G. Madejski,[13] C. Panagiotou,[8] P. O. Petrucci,[14] J. Podgorny,[3,5,15] S. Puccetti,[6] F. Tombesi,[16,17,18] A. Veledina,[19,20,21] W. Zhang,[22] I. Agudo,[23] L. A. Antonelli,[6,7] M. Bachetti,[24] W. H. Baumgartner,[25] R. Bellazzini,[9] S. D. Bongiorno,[25] R. Bonino,[26,27] A. Brez,[9] N. Bucciantini,[28,29,30] F. Capitanio,[2] S. Castellano,[9] E. Cavazzuti,[1] S. Ciprini,[6,17] E. Costa,[2] E. Del Monte,[2] N. Di Lalla,[13] A. Di Marco,[2] I. Donnarumma,[1] V. Doroshenko,[21,31] S. R. Ehlert,[25] T. Enoto,[32] Y. Evangelista,[2] S. Fabiani,[2] R. Ferrazzoli,[2] J. A. Garcia,[33] S. Gunji,[34] K. Hayashida,[35] J. Heyl,[36] W. Iwakiri,[37] S. G. Jorstad,[38,39] T. Kitaguchi,[32] J. J. Kolodziejczak,[25] F. La Monaca,[2] L. Latronico,[26] I. Liodakis,[40] S. Maldera,[26] A. Manfreda,[9] A. P. Marscher,[38] I. Mitsuishi,[41] T. Mizuno,[42] C.-Y. Ng,[43] S. L. O'Dell,[25] N. Omodei,[13] C. Oppedisano,[26] A. Papitto,[7] G. G. Pavlov,[44] A. L. Peirson,[13] M. Perri,[6,7] M. Pesce-Rollins,[9] M. Pilia,[24] A. Possenti,[24] J. Poutanen,[19,21] B. D. Ramsey,[25] J. Rankin,[2] A. Ratheesh,[2] R. W. Romani,[13] C. Sgrš,[9] P. Slane,[45] P. Soffitta,[2] G. Spandre,[9] T. Tamagawa,[32] F. Tavecchio,[46] R. Taverna,[47] Y. Tawara,[41] A. F. Tennant,[25] N. E. Thomas,[25] A. Trois,[24] S. S. Tsygankov,[19,21] R. Turolla,[47,48] J. Vink,[49] M. C. Weisskopf,[25] K. Wu,[48] F. Xie[2,50] and S. Zane[48]

Affiliations are listed at the end of the paper

Accepted 2022 September 12. Received 2022 September 6; in original form 2022 July 21

ABSTRACT

We report on the first observation of a radio-quiet active galactic nucleus (AGN) in polarized X-rays: the Seyfert 1.9 galaxy MCG-05-23-16. This source was pointed at with the *Imaging X-ray Polarimetry Explorer* (*IXPE*) starting on 2022 May 14 for a net observing time of 486 ks, simultaneously with XMM-*Newton* (58 ks) and *NuSTAR* (83 ks). A polarization degree Π smaller than 4.7 per cent (at the 99 per cent confidence level) is derived in the 2–8 keV energy range, where emission is dominated by the primary component ascribed to the hot corona. The broad-band spectrum, inferred from a simultaneous fit to the *IXPE*, *NuSTAR*, and XMM-*Newton* data, is well reproduced by a power law with photon index $\Gamma = 1.85 \pm 0.01$ and a high-energy cutoff $E_C = 120 \pm 15$ keV. A comparison with Monte Carlo simulations shows that a lamp-post and a conical geometry of the corona are consistent with the observed upper limit, a slab geometry is allowed only if the inclination angle of the system is less than 50°.

Key words: galaxies: active – galaxies: individual: MCG-05-23-16 - polarization – galaxies: Seyfert.

1 INTRODUCTION

It is now widely accepted that the primary X-ray emission of Seyfert galaxies is produced by multiple upscattering events of cool photons by hot electrons: the Comptonization process (Sunyaev & Titarchuk 1980; Zdziarski, Poutanen & Johnson 2000). However, the energy supply of this medium and the conditions leading to a formation of the hot plasma close to the black hole are debated. The physical picture of plasma fuelling through the gravitational energy transformation greatly depends on the geometry and size of the hot medium. In one scenario, the energy dissipation (and electron heating) is distributed over a large volume, with characteristic sizes ∼10–100 R_g (where $R_g = GM/c^2$ is the gravitational radius, G is the gravitational constant, M is the black hole mass, and c is the speed of light). Early studies considered the so-called two-phase disc-corona model, where the hot medium was assumed to be distributed above the cold accretion disc (Haardt & Maraschi 1991, 1993), and presumably energized by some disc instability, likely of magnetic origin (Merloni 2003). However, the X-ray spectral shape appears too soft in this geometry, once the feedback of the heated accretion disc is taken into account (Stern et al. 1995), unless the disc is highly ionized (Malzac, Dumont & Mouchet 2005; Poutanen, Veledina & Zdziarski 2018), the corona is patchy (Haardt, Maraschi & Ghisellini 1994; Stern et al. 1995;

★ E-mail: andrea.marinucci@asi.it

© 2022 The Author(s)
Published by Oxford University Press on behalf of Royal Astronomical Society

Downloaded from https://academic.oup.com/mnras/article/516/4/5907/6731657 by INIST-CNRS INEE INSB user on 06 July 2023

Poutanen & Svensson 1996) or it is outflowing (Beloborodov 1999). Hot accretion flows, replacing the cold disc in the inner parts, have also been proposed (Shapiro, Lightman & Eardley 1976; Ichimaru 1977; Narayan, Yi & Mahadevan 1995; Yuan & Zdziarski 2004; Yuan & Narayan 2014). The seed photons for Comptonization in these models come either from the truncated accretion disc (Zdziarski 1998) or from the synchrotron photons produced internally in the hot flow (Özel, Psaltis & Narayan 2000; Veledina, Vurm & Poutanen 2011; Niedźwiecki, Xie & Zdziarski 2012).

On the other hand, in a *lamp-post* geometry, the primary X-ray emission is assumed to be coming from a compact source (∼1–10 R_g), located on the accretion disc axis (Fabian et al. 2017b) and could be associated with an aborted jet (Ghisellini, Haardt & Matt 2004).

Spectroscopic analyses have in principle the capability to constrain the coronal geometry but, even the best available observations provided by *NuSTAR*, while good enough to measure the physical coronal parameters like the optical depth and the temperature, are not able to distinguish statistically among different geometries (Tortosa et al. 2018; Middei et al. 2019).

A very promising and powerful tool to assess the coronal geometry is reverberation mapping of the corona-disc system (Uttley et al. 2014, and references therein). In fact, the disc response to the corona illumination depends also on the geometry of the latter (Wilkins et al. 2016). However, to fully exploit this technique, observations with the next-generation X-ray observatories such as *eXTP* and *Athena* are required (Dovciak et al. 2013; De Rosa et al. 2019), even if very long XMM-*Newton* observations can already deliver some results (Fabian et al. 2017a).

X-ray polarization provides an independent tool to constrain the coronal geometry. Polarization, in fact, is extremely sensitive to the geometry of the emitting matter and of the photon field (Schnittman & Krolik 2010; Beheshtipour, Krawczynski & Malzac 2017; Tamborra et al. 2018; Zhang, Dovčiak & Bursa 2019). With the aim to constrain its coronal geometry, the *Imaging X-ray Polarimetry Explorer* (*IXPE*: Weisskopf et al. 2016) observed the bright Seyfert galaxy MCG-05-23-16.

MCG-05-23-16 is a nearby ($z = 0.0085$ or 36 Mpc, Wegner et al. 2003) Seyfert 1.9 galaxy with broad emission lines in the near-infrared (Goodrich, Veilleux & Hill 1994). It has been extensively observed in X-rays (Weaver et al. 1997; Perola et al. 2002; Balestra, Bianchi & Matt 2004; Braito et al. 2007; Reeves et al. 2007; Beckmann et al. 2008; Molina et al. 2013), showing a moderate cold absorption ($N_H \sim 10^{22}$ cm^{-2}). Recently, *NuSTAR* observations were able to constrain the high energy cutoff ($E_C \sim$ 100–160 keV, variable on a time-scale of ∼100 ks) and therefore the coronal physical parameters kT_e and τ (Baloković et al. 2015; Zoghbi et al. 2017). X-ray reverberation features have also been detected with XMM-*Newton* in this source (Zoghbi et al. 2013; Kara et al. 2016).

In the optical and near-infrared wavelengths (0.4–2.2 μm), the source exhibits a low continuum linear polarization degree (1–2 per cent) and a polarized flux density, which increases with wavelength, a possible sign of Compton scattering or a different non-thermal component at work (Brindle et al. 1990).

With a 2–10 keV flux of (7–10) × 10^{-11} erg cm^{-2} s^{-1} (Mattson & Weaver 2004), MCG-05-23-16 is one of the brightest Seyfert galaxies, only moderately variable on both short and long time-scales, with a relatively simple spectrum (no significant absorption in the *IXPE* band) and well-measured coronal parameters. It is therefore the ideal target to search for polarization signatures of the coronal geometry in radio-quiet active galactic nucleus (AGN). The paper is organized as follows: in Section 2, we discuss the data reduction procedure, while in Section 3 we present the spectropolarimetric analyses. Our results are then discussed and summarized in Sections 4 and 5.

2 OBSERVATIONS AND DATA REDUCTION

IXPE (Weisskopf et al. 2022) observed MCG-05-23-16 starting on 2022 May 14 with its three Detector Units (DU), for a net exposure time of 47 ks. The pointing at the source started again on May 21, for additional 439 ks. Cleaned level 2 event files were produced and calibrated using standard filtering criteria with the dedicated FTOOLS tasks and the latest calibration files available in the *IXPE* calibration data base (CALDB 20211118). *I*, *Q*, and *U* Stokes background spectra were extracted from source-free circular regions with a radius of 100 arcsec. Extraction radii for the *I* Stokes spectra of the source were computed via an iterative process, which leads to the maximization of the signal-to-noise ratio (SNR) in the 2–8 keV energy band, similar to the approach described in Piconcelli et al. (2004). We therefore adopted circular regions centred on the source with radii of 62, 57, and 62 arcsec for DU1, DU2, and DU3, respectively. The net exposure times are 485.7 ks and the same extraction radii were then applied to the *Q* and *U* Stokes spectra. We used a constant energy binning of 0.2 keV for *Q* and *U* Stokes spectra and required a SNR higher than 5 in each spectral channel, in the intensity spectra. *I*, *Q*, and *U* Stokes spectra from the three DUs are always fitted independently in the following, but we will plot them together using the SETP GROUP command in XSPEC, for the sake of visual clarity. Background represents the 2.0 per cent, 1.8 per cent, and 2.1 per cent of the total DU1, DU2, and DU3 *I* spectra, respectively. The summed background-subtracted light curves show an average count rate $C_{2\text{–}8\,\mathrm{keV}} = 0.525 \pm 0.002$ cts s^{-1} with a level of variability of ∼20–30 per cent, in the range 0.33–0.79 cts s^{-1}.

XMM-*Newton* started its observation on 2022 May 21 for 83 ks of elapsed time with the EPIC CCD cameras: the pn (Strüder et al. 2001) and the two MOS (Turner et al. 2001), operated in small window and medium filter mode. Data from the MOS detectors are not included in our analysis due to pile-up. The data from the pn camera show no significant pile-up as indicated by the EPATPLOT output. The extraction radii and the optimal time cuts for flaring particle background were computed with SAS 20 (Gabriel et al. 2004) with the same SNR maximization procedure reported above. The resulting optimal extraction radii for the source and the background spectra are 40 and 50 arcsec, respectively. The net exposure time for the pn time-averaged spectrum is 58.1 ks. The 0.5–10 keV background-subtracted light curve show an average count rate $C_{0.5\text{–}10\,\mathrm{keV}} = 8.55 \pm 0.01$ cts s^{-1}.

NuSTAR (Harrison et al. 2013) observed MCG-05-23-16 simultaneously to XMM-*Newton*, with its two co-aligned X-ray telescopes with corresponding Focal Plane Module A (FPMA) and B (FPMB). The total elapsed time is 171.4 ks. The Level 1 data products were processed with the *NuSTAR* Data Analysis Software (NUSTARDAS) package (v. 2.1.2). Cleaned event files (level 2 data products) were produced and calibrated using standard filtering criteria with the NUPIPELINE task and the latest calibration files available in the *NuSTAR* calibration data base (CALDB 20220510). Extraction radii for the source and background spectra were 40 and 60 arcsec, FPMA spectra were binned in order not to oversample the instrumental resolution more than a factor of 2.5 and to have a SNR greater than 5 in each spectral channel, the same energy binning was then applied to the FPMB spectra. The net observing times for the FPMA and the FPMB data sets are 83.4 and 83 ks, respectively. The

Downloaded from https://academic.oup.com/mnras/article/516/4/5907/6731657 by INIST-CNRS INEE INSB user on 06 July 2023

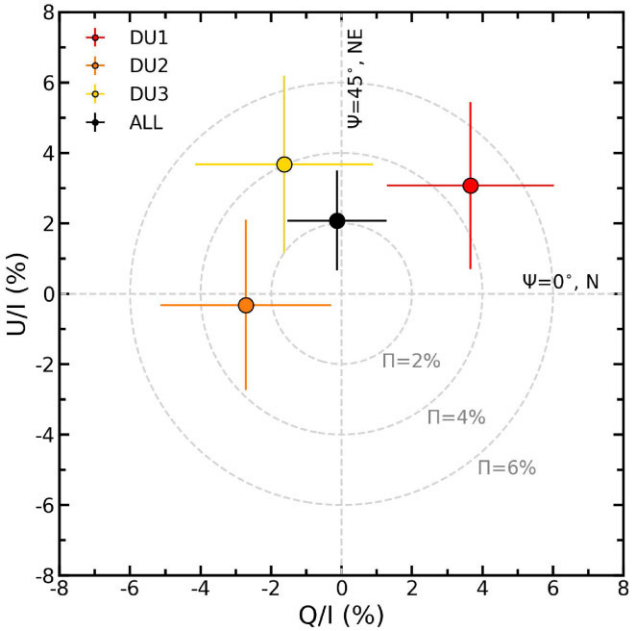

Figure 1. Normalized *U*/*I* and *Q*/*I* Stokes parameters are shown, calculated using the full 2–8 keV *IXPE* band. Uncertainties are reported at the 68 per cent c.l.

summed background-subtracted FPMA and FPMB light curves show an average count rate $C_{3\text{–}79\,\mathrm{keV}} = 8.27 \pm 0.02$ cts s^{-1}.

We adopt the cosmological parameters $H_0 = 70$ km s^{-1} Mpc^{-1}, $\Omega_\Lambda = 0.73$, and $\Omega_\mathrm{m} = 0.27$, i.e. the default ones in XSPEC 12.12.1 (Arnaud 1996). Errors correspond to the 90 per cent confidence level for one interesting parameter ($\Delta\chi^2 = 2.7$), if not stated otherwise.

3 DATA ANALYSIS

3.1 *IXPE* polarimetric analysis

We start investigating the polarized signal from MCG-05-23-16 by analysing its polarization cubes, which are the simplest data structures holding polarization information. They can be created using IXPEOBSSIM (version 26.3.3: Baldini et al. 2022). This applies the Kislat et al. (2015) formalism to a user-defined set of events to compute the Stokes parameters, the Minimum Detectable Polarization (MDP; Elsner, O'Dell & Weisskopf 2012), the polarization degree, the polarization angle, and the associated uncertainties. In our case, we created one polarization cube for each DU and then one combining the three, using the whole 2–8 keV band. Fig. 1 shows the normalized *U*/*I* and *Q*/*I* Stokes parameters, in which polarization cubes from the background have been taken into account. We find $U/I = 2.1 \pm 1.4$ per cent and $Q/I = -0.1 \pm 1.4$ per cent (using 68 per cent c.l. on one single parameter). We do not constrain any energy dependence of the polarization properties.

3.2 XMM-*Newton*, *NuSTAR* and *IXPE* spectro-polarimetric analysis

We started modelling the simultaneous 2–10 keV XMM-*Newton* and 3–79 keV *NuSTAR* spectra of MCG-05-23-16 with a model composed of an absorbed cut-off power law (ZTBABS × CUTOFFPL in XSPEC) and a Compton reflection component (XILLVER; García et al. 2013). The former reproduces the primary continuum of the source while the latter takes into account reflection off neutral, distant material. Galactic absorption is modelled with TBABS, using a column density $N_\mathrm{H} = 7.8 \times 10^{20}$ cm^{-2} (HI4PI Collaboration 2016) and multiplicative constants take into account cross-calibration uncertainties between the FPMA, the FPMB, and EPIC pn. The photon index and cut-off energy of the reflection continuum is linked to the one of the primary continuum, iron abundance is fixed to the solar one, and the inclination angle to $\theta = 30°$. The resulting χ^2/dof is good (785/628) but some residuals appear at ∼6 keV.[1] This could be indicative of a second iron Kα component, smeared by relativistic effects in the inner regions of the accretion disc. Indeed, when compared with old XMM data, the residuals are perfectly consistent with the ones presented in Braito et al. (2007). A further spectral component is therefore included: (KERRDISK; Brenneman & Reynolds 2006). The black hole spin is fixed to $a = 0.998$, the emissivity to $\epsilon(r) = r^{-3}$, the rest-frame energy of the emission line at 6.4 keV, and the inner radius of the disc to $R_\mathrm{in} = 37\,R_\mathrm{g}$ (as reported in the simultaneous XMM + *Suzaku* analysis: Reeves et al. 2007). We obtain a best-fitting χ^2/dof = 683/625 (Fig. 2) and an inclination angle $\theta = 48^{+12°}_{-8}$. We note that a more detailed modelling of the reflection features from the accretion disc is needed to better determine the total Compton reflection fraction *R*. However, this is beyond the scope of this work and it will be presented in a forthcoming paper.

We then included *IXPE I* Stokes spectra to the XMM and *NuSTAR* fit. We followed the formalism discussed in Strohmayer (2017) and used the weighted analysis method presented in Di Marco et al. (2022; parameter STOKES = NEFF in XSELECT). We obtain a χ^2/dof = 1378/1000 due to presence of large residuals at the low and high energies in the *IXPE I* spectra. This has already been observed in other bright sources and can be likely explained in terms of calibration issues (Krawczynski et al. 2022; Taverna et al. 2022). We therefore modified the response files gains in the *I* spectra (using GAIN FIT command) and obtained a χ^2/dof = 1055/994. We then included the *Q* and *U* Stokes spectra and linked their gain parameters to the ones of the *I* spectra. Cross-calibration constants are included and the three spectral components of the model are convolved with the polarization model POLCONST. Two parameters can be then be inferred for each spectral component: the polarization degree Π and angle Ψ, both constant functions of the energy. The polarization degree and angle associated to the nuclear continuum are left free to vary while the ones associated to the other spectral components are fixed to $\Pi = 0$ per cent and $\Psi = 0°$. We will state *a posteriori* that the fit is insensitive to these values. We retrieve the photon index $\Gamma = 1.85 \pm 0.01$ and the cut-off energy $E_\mathrm{C} = 120 \pm 15$ keV, in agreement with previously reported values (Baloković et al. 2015; Zoghbi et al. 2017). The best spectropolarimetric joint fit provides, at the 99 per cent c.l. (for one single parameter of interest, $\Delta\chi^2 = 6.63$), only an upper limit on the polarization degree $\Pi = 4.7$ per cent. It is worth noting that the MDP and the upper limit for the polarization degree are not directly comparable. The value in Ursini et al. (2022) is the MDP of the measurement, which is the maximum polarization expected to be measured for an unpolarized source at the 99 per cent confidence level. In other words, the MDP is the level at which one can accept or reject the hypothesis that the observed signal can be generated by an unpolarized source. Instead, the upper limit quoted

[1]The inferred energy of the Fe Kα line in the pn spectrum is not consistent with 6.4 keV, and we therefore added a VASHIFT component in the model. We retrieve $v = 2230^{+510}_{-550}$ km s^{-1}. Since this effect is not found in the MOS spectra, we conclude that is likely due to calibration issues in the pn.

Downloaded from https://academic.oup.com/mnras/article/516/4/5907/6731657 by INIST-CNRS INEE INSB user on 06 July 2023

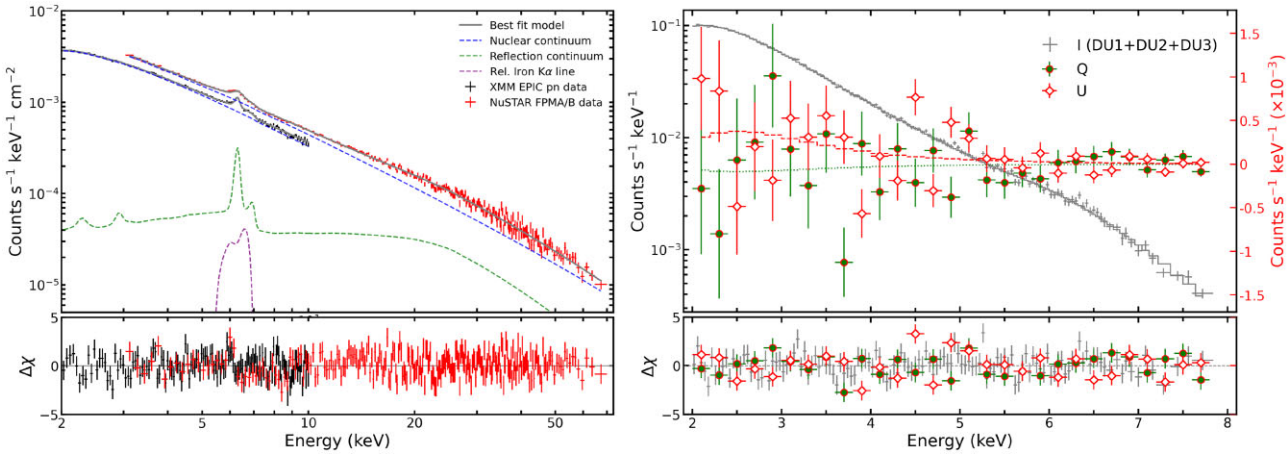

Figure 2. Left-hand panel: the simultaneous EPIC pn and the grouped *NuSTAR* FPMA and FPMB spectra of MCG-05-23-16 divided by the relative effective area are shown with residuals. The best-fitting model is shown as a solid grey line and the different components as dashed lines. Right-hand panel: *IXPE I* (grey circles), *Q* (green circles,) and *U* (red empty circles) grouped Stokes spectra are shown with residuals, along with the corresponding best-fitting models. Note the different scales on the *y*-axes for *I* and *Q*/*U* data.

above is the upper bound of the interval in which the measured polarization degree varies at the 99 per cent confidence level. The difference with respect to the MDP = 2 per cent value presented in Ursini et al. (2022) is mainly due to the lower flux of the source, to the vignetting effects at the time of the IXPE pointing and to the inclusion of the energy dependence of the instrument sensitivity. The contour plots of the best-fitting polarization degree Π and angle Ψ are shown in Fig. 3. If the cut-off power law is substituted by the Comptonization model COMPPS (Poutanen & Svensson 1996) an electron temperature $kT_e = 25 \pm 2$ keV and optical depth $\tau = 1.27 \pm 0.08$ are retrieved, assuming a slab geometry (χ^2/dof = 1248/1169).

On theoretical grounds, the Compton reflection continuum is expected to be moderately polarized but the iron Kα fluorescence emission line arising from the same scattering material is not (as shown in Goosmann & Matt 2011; Marin 2018). We also note that scattering from distant AGN components do not significantly impact the measured polarization due to their low contribution in this energy band (Marin, Dovčiak & Kammoun 2018). However, we also tried to leave the polarization degree of the XILLVER and KERRDISK components free to vary in the fit. No statistically significant improvement is found (χ^2/dof = 1250/1169) and the fit is insensitive to these two parameters.

4 DISCUSSION

Several radio-loud AGNs have been observed in the first *IXPE* months of operations and a highly significant polarized signal has been measured in two blazars so far, due to synchrotron emission in the jet. On the other hand, polarized X-rays produced in radio quiet sources are thought to be produced by the inverse Compton mechanism, occurring within tens of gravitational radii from the central black hole. Different geometries of the scattering medium, depending on the degree of asymmetry, will result in a different degree of polarization.

MCG-05-23-16 is the first radio-quiet AGN observed by *IXPE* and the nuclear power-law component, ascribed to the hot corona, contributes to the 94 ± 3 per cent of the 2–8 keV flux. We found that the best spectropolarimetric fit of the simultaneous *IXPE-NuSTAR*-XMM data provides only, at the 99 per cent c.l., an upper limit Π = 4.7 per cent. Three different, simple geometries for the hot corona in

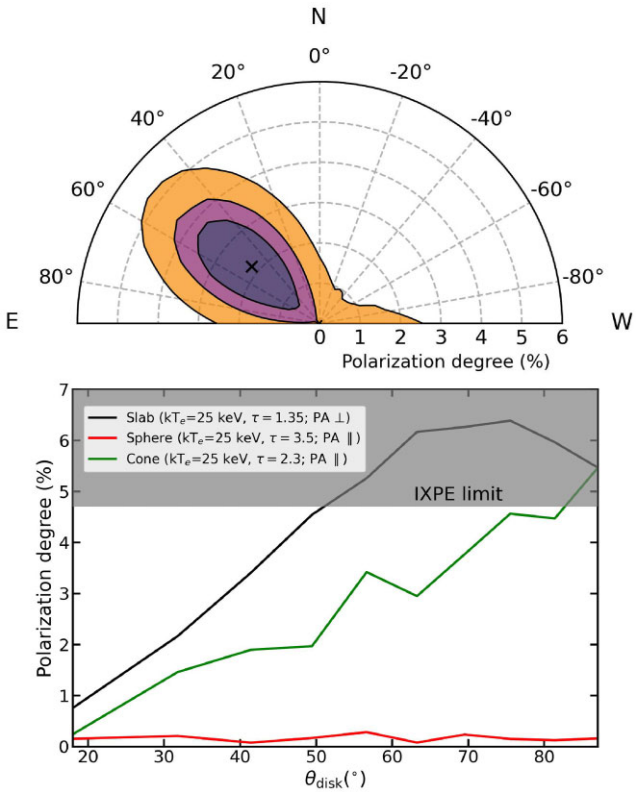

Figure 3. Top-panel: contour plot of the polarization degree Π and angle Ψ associated to the primary power law component. Purple-, pink-, and orange-shaded regions indicate 68 per cent, 90 per cent, and 99 per cent confidence levels for two parameters of interest, respectively. Bottom-panel: Monte Carlo simulations performed with the Comptonization code MONK. The input coronal parameters kT_e, τ correspond to the spectral shape reported in Table 1 and the polarization angle is reported with respect to the accretion disc plane.

this AGN have been recently explored in Ursini et al. (2022), with the Comptonization code MONK (Zhang et al. 2019). Fig. 3 shows the results with input coronal temperatures $kT_e = 25$ keV and different Thomson optical depths τ, which correspond to the spectral shape of

Downloaded from https://academic.oup.com/mnras/article/516/4/5907/6731657 by INIST-CNRS INEE INSB user on 06 July 2023

Table 1. Best-fitting parameters from the joint fit. Normalization units are in photons keV^{-1} cm^{-2} s^{-1}. R is the reflection fraction measured as the ratio between the Compton reflection and the primary component fluxes between 20 and 40 keV. The 2–10 keV flux is retrieved from the EPIC-pn data.

Parameter	Best-fitting values		
CUTOFF POWER LAW			
$N_{\rm H}$ (cm^{-2})	$(1.35 \pm 0.05) \times 10^{22}$		
Γ	1.85 ± 0.01		
$E_{\rm C}$ (keV)	120 ± 15		
N	$(2.60 \pm 0.05) \times 10^{-2}$		
Π (per cent)	2.2 ± 1.7		
Ψ (°)	50 ± 25		
XILLVER			
R	0.30 ± 0.05		
N	$2.14^{+0.4}_{-0.1} \times 10^{-2}$		
Π (per cent)	–		
Ψ (°)	–		
KERRDISK			
θ (°)	48^{+12}_{-8}		
N	$(3.9\pm^{+0.8}_{-0.5}) \times 10^{-5}$		
Π (per cent)	–		
Ψ (°)	–		
χ^2/dof	1250/1169		
F_{2-10} (erg cm^{-2} s^{-1})	$(7.45 \pm 0.05) \times 10^{-11}$		
L_{2-10} (erg s^{-1})	$(1.20 \pm 0.02) \times 10^{43}$		
CROSS-CALIBRATIONS			
CONSTANTS		GAIN	
$C_{\text{pn-DU1}}$	$1.09^{+0.02}_{-0.01}$	$\alpha_{\rm DU1}$	0.953 ± 0.009
$C_{\text{pn-DU2}}$	1.06 ± 0.02	$\beta_{\rm DU1}$	0.07 ± 0.03
$C_{\text{pn-DU3}}$	0.97 ± 0.02	$\alpha_{\rm DU2}$	$0.963^{+0.007}_{-0.009}$
$C_{\text{pn-FPMA}}$	1.39 ± 0.01	$\beta_{\rm DU2}$	0.04 ± 0.03
$C_{\text{pn-FPMB}}$	1.43 ± 0.01	$\alpha_{\rm DU3}$	$0.951^{+0.009}_{-0.007}$
		$\beta_{\rm DU3}$	$0.07^{+0.03}_{-0.04}$

the continuum reported in Table 1. The three coronal geometries are: a slab sandwiching the accretion disc, a spherical lamp-post on the symmetry axis, and a truncated cone in outflow to describe the base of a failed jet. The geometrical parameters for the simulations shown in Fig. 3 are as follows. The slab corona fully covers a truncated disc with an inner radius of 30 R_g. The spherical lamp-post has a radius of 10 R_g and a height above the disc of 30 R_g. As for the truncated cone, the distance between the lower base and the disc and the vertical thickness are both of 20 R_g, while the semi-aperture is 30°, and the outflow velocity is 0.3c. Among these geometries, the slab corona is the only one that gives a polarization vector perpendicular to the disc plane, the other two predicting it to be parallel to the accretion disc. However, as already noted, in the two-phase disc-corona scenario (Haardt & Maraschi 1991, 1993) rather steep spectra are predicted, and the observed value of 1.85 for the photon index is possible only for quite a low-optical depth $\tau \lesssim 0.2$ and high-temperature $kT_{\rm e} \gtrsim$ 130 keV (Stern et al. 1995) or a highly ionized disc (Malzac et al. 2005; Poutanen et al. 2018). Other possible solutions are a patchy, rather than homogeneous, corona (Haardt et al. 1994; Poutanen et al. 2018) or the inner hot optically thin flow within the truncated cold accretion disc (Yuan & Narayan 2014). Detailed calculations of these scenarios are beyond the scope of the paper and will be deferred to future works. We note, however, that for a small height-to-radius ratio, the hot flow polarimetric properties in the *IXPE* range are similar to those of the slab-corona model. Finally, we note that the polarization angle for the three geometries does not significantly vary for different input kT_e and τ values, while the absolute value of the polarization degree can change. However, this does not impact much on the relative differences between the three geometries.

VLA observations at 8.4 GHz of the source showed a possible elongation at the position angle PA $\simeq 169°$ east of north (Mundell et al. 2009) while *Hubble Space Telescope* WFPC2 images revealed [O III] emission in PA $\simeq 40°$ (Ferruit, Wilson & Mulchaey 2000). The 90 per cent c.l. contour plot shows that the polarization angle is roughly aligned with the [O III] emitting region, which likely traces the narrow-line region (NLR) in this object. Assuming that the accretion disc is perpendicular to the NLR, a flat configuration of the emitting matter would produce such a polarization angle, similar to what observed in the X-ray binary Cyg X-1 (Krawczynski et al. 2022). Of course, given the low significance of this result, it must be taken as no more than suggestive, needing more data for a confirmation. Highly inclined slab geometries (with $\theta \gtrsim 50°$) can be ruled out and our estimate of $\theta = 48^{+12°}_{-8}$, from the broad iron Kα profile, does not provide further constraints on the hot coronal geometry.

5 CONCLUSIONS

The launch of *IXPE*, on 2021 December 9, opened a new observing window on the study of supermassive black holes, and MCG-05-23-16 is the perfect candidate to investigate the hot corona close to the supermassive black hole. Simultaneously observed with *IXPE*, XMM-*Newton*, and *NuSTAR* in 2022 May, the source showed a low level of neutral absorption along the line of sight ($N_{\rm H} = 1.35 \pm 0.05 \times 10^{22}$ cm^{-2}), a modest level of Compton reflection ($R = 0.30 \pm 0.05$), and broad relativistic iron Kα emission line. This translates into a power-law continuum that largely dominates the total flux in the 2–8 keV *IXPE* band ($F_{\rm pow}/F_{\rm tot} = 94 \pm 3$ per cent), and when it is convolved with a constant polarization model, we obtain a 99 per cent c.l. upper limit to the polarization fraction of 4.7 per cent. This result is consistent with a spherical ('lamp-post') and a conical geometry of the corona, while for a slab corona (with $kT_e = 25$ keV and $\tau = 1.35$) it implies an inclination angle less than 50°.

ACKNOWLEDGEMENTS

We thank the anonymous referee for her/his comments and suggestions, which greatly improved the clarity of the paper. The *IXPE* is a joint US and Italian mission. The US contribution is supported by the National Aeronautics and Space Administration (NASA) and led and managed by its Marshall Space Flight Center (MSFC), with industry partner Ball Aerospace (contract NNM15AA18C). The Italian contribution is supported by the Italian Space Agency (ASI) through contract ASI-OHBI-2017-12-I.0, agreements ASI-INAF-2017-12-H0 and ASI-INFN-2017.13-H0, and its Space Science Data Center (SSDC), and by the Istituto Nazionale di Astrofisica (INAF) and the Istituto Nazionale di Fisica Nucleare (INFN) in Italy. This research used data products provided by the *IXPE* Team (MSFC, SSDC, INAF, and INFN) and distributed with additional software tools by the High-Energy Astrophysics Science Archive Research Center (HEASARC), at NASA Goddard Space Flight Center (GSFC). Part of the French contribution is supported by the Scientific Research National Center (CNRS) and the French spatial agency (CNES). MD, VK, and JP thank for the support from the GACR project 21-06825X and the institutional support from RVO:67985815. IA acknowledges financial support from the

Downloaded from https://academic.oup.com/mnras/article/516/4/5907/6731657 by INIST-CNRS INEE INSB user on 06 July 2023

Spanish 'Ministerio de Ciencia e Innovación' (MCINN) through the 'Center of Excellence Severo Ochoa' award for the Instituto de Astrofísica de Andalucía-CSIC (SEV-2017-0709) and through grants AYA2016-80889-P and PID2019-107847RB-C44.

DATA AVAILABILITY

The data analysed in this work are either publicly available at the HEASARC data base or available from the corresponding author upon request.

REFERENCES

Arnaud K. A., 1996, in ASP Conf. Ser. Vol.101, Astronomical Data Analysis Software and Systems V. Astron. Soc. Pac., San Francisco, p. 17
Baldini L., Bucciantini N., Di Lalla N., Ehlert S. R., Manfreda A., Omodei N., Pesce-Rollins M., Sgrò C., 2022, preprint (arXiv:2203.06384)
Balestra I., Bianchi S., Matt G., 2004, A&A, 415, 437
Baloković M. et al., 2015, ApJ, 800, 62
Beckmann V., Courvoisier T. J. L., Gehrels N., Lubiński P., Malzac J., Petrucci P. O., Shrader C. R., Soldi S., 2008, A&A, 492, 93
Beheshtipour B., Krawczynski H., Malzac J., 2017, ApJ, 850, 14
Beloborodov A. M., 1999, ApJ, 510, L123
Braito V. et al., 2007, ApJ, 670, 978
Brenneman L. W., Reynolds C. S., 2006, ApJ, 652, 1028
Brindle C., Hough J. H., Bailey J. A., Axon D. J., Ward M. J., Sparks W. B., McLean I. S., 1990, MNRAS, 244, 604
De Rosa A. et al., 2019, Sci. China Phys. Mech. Astron., 62, 29504
Di Marco A. et al., 2022, AJ, 163, 170
Dovciak M. et al., 2013, preprint (arXiv:1306.2331)
Elsner R. F., O'Dell S. L., Weisskopf M. C., 2012, Proc. SPIE Conf. Ser. Vol. 8443, Space Telescopes and Instrumentation 2012: Ultraviolet to Gamma Ray. p. 84434N , preprint (arXiv:1208.0610)
Fabian A. C., Alston W. N., Cackett E. M., Kara E., Uttley P., Wilkins D. R., 2017a, Astron. Nachr., 338, 269
Fabian A. C., Lohfink A., Belmont R., Malzac J., Coppi P., 2017b, MNRAS, 467, 2566
Ferruit P., Wilson A. S., Mulchaey J., 2000, ApJS, 128, 139
Gabriel C. et al., 2004, in Ochsenbein F., Allen M. G., Egret D., eds, ASP Conf. Ser. Vol. 314, Astronomical Data Analysis Software and Systems (ADASS) XIII. Astron. Soc. Pac., San Francisco, p. 759
García J., Dauser T., Reynolds C. S., Kallman T. R., McClintock J. E., Wilms J., Eikmann W., 2013, ApJ, 768, 146
Ghisellini G., Haardt F., Matt G., 2004, A&A, 413, 535
Goodrich R. W., Veilleux S., Hill G. J., 1994, ApJ, 422, 521
Goosmann R. W., Matt G., 2011, MNRAS, 415, 3119
Haardt F., Maraschi L., 1991, ApJ, 380, L51
Haardt F., Maraschi L., 1993, ApJ, 413, 507
Haardt F., Maraschi L., Ghisellini G., 1994, ApJ, 432, L95
Harrison F. A. et al., 2013, ApJ, 770, 103
HI4PI Collaboration, 2016, A&A, 594, A116
Ichimaru S., 1977, ApJ, 214, 840
Kara E., Alston W. N., Fabian A. C., Cackett E. M., Uttley P., Reynolds C. S., Zoghbi A., 2016, MNRAS, 462, 511
Kislat F., Clark B., Beilicke M., Krawczynski H., 2015, Astropart. Phys., 68, 45
Krawczynski H. et al., 2022, preprint (arXiv:2206.09972)
Malzac J., Dumont A. M., Mouchet M., 2005, A&A, 430, 761
Marin F., 2018, A&A, 615, A171
Marin F., Dovčiak M., Kammoun E. S., 2018, MNRAS, 478, 950
Mattson B. J., Weaver K. A., 2004, ApJ, 601, 771
Merloni A., 2003, MNRAS, 341, 1051
Middei R., Bianchi S., Marinucci A., Matt G., Petrucci P. O., Tamborra F., Tortosa A., 2019, A&A, 630, A131
Molina M., Bassani L., Malizia A., Stephen J. B., Bird A. J., Bazzano A., Ubertini P., 2013, MNRAS, 433, 1687
Mundell C. G., Ferruit P., Nagar N., Wilson A. S., 2009, ApJ, 703, 802
Narayan R., Yi I., Mahadevan R., 1995, Nature, 374, 623
Niedźwiecki A., Xie F.-G., Zdziarski A. A., 2012, MNRAS, 420, 1195
Perola G. C., Matt G., Cappi M., Fiore F., Guainazzi M., Maraschi L., Petrucci P. O., Piro L., 2002, A&A, 389, 802
Piconcelli E., Jimenez-Bailón E., Guainazzi M., Schartel N., Rodríguez-Pascual P. M., Santos-Lleó M., 2004, MNRAS, 351, 161
Poutanen J., Svensson R., 1996, ApJ, 470, 249
Poutanen J., Veledina A., Zdziarski A. A., 2018, A&A, 614, A79
Reeves J. N. et al., 2007, PASJ, 59, 301
Schnittman J. D., Krolik J. H., 2010, ApJ, 712, 908
Shapiro S. L., Lightman A. P., Eardley D. M., 1976, ApJ, 204, 187
Stern B. E., Poutanen J., Svensson R., Sikora M., Begelman M. C., 1995, ApJ, 449, L13
Strohmayer T. E., 2017, ApJ, 838, 72
Strüder L. et al., 2001, A&A, 365, L18
Sunyaev R. A., Titarchuk L. G., 1980, A&A, 86, 121
Tamborra F., Matt G., Bianchi S., Dovčiak M., 2018, A&A, 619, A105
Taverna R. et al., 2022, preprint (arXiv:2205.08898)
Tortosa A., Bianchi S., Marinucci A., Matt G., Petrucci P. O., 2018, A&A, 614, A37
Turner M. J. L. et al., 2001, A&A, 365, L27
Ursini F., Matt G., Bianchi S., Marinucci A., Dovčiak M., Zhang W., 2022, MNRAS, 510, 3674
Uttley P., Cackett E. M., Fabian A. C., Kara E., Wilkins D. R., 2014, A&AR, 22, 72
Veledina A., Vurm I., Poutanen J., 2011, MNRAS, 414, 3330
Weaver K. A., Yaqoob T., Mushotzky R. F., Nousek J., Hayashi I., Koyama K., 1997, ApJ, 474, 675
Wegner G. et al., 2003, AJ, 126, 2268
Weisskopf M. C. et al., 2016, Results Phys., 6, 1179
Weisskopf M. C. et al., 2022, J. Astron. Telesc. Instrum. Syst., 8, 026002
Wilkins D. R., Cackett E. M., Fabian A. C., Reynolds C. S., 2016, MNRAS, 458, 200
Yuan F., Narayan R., 2014, ARA&A, 52, 529
Yuan F., Zdziarski A. A., 2004, MNRAS, 354, 953
Zdziarski A. A., 1998, MNRAS, 296, L51
Zdziarski A. A., Poutanen J., Johnson W. N., 2000, ApJ, 542, 703
Zhang W., Dovčiak M., Bursa M., 2019, ApJ, 875, 148
Zoghbi A., Reynolds C., Cackett E. M., Miniutti G., Kara E., Fabian A. C., 2013, ApJ, 767, 121
Zoghbi A. et al., 2017, ApJ, 836, 2
Özel F., Psaltis D., Narayan R., 2000, ApJ, 541, 234

[1]*ASI - Agenzia Spaziale Italiana, Via del Politecnico snc, I-00133 Roma, Italy*
[2]*INAF Istituto di Astrofisica e Planetologia Spaziali, Via del Fosso del Cavaliere 100, I-00133 Roma, Italy*
[3]*Astronomical Institute of the Czech Academy of Sciences, Bocní II 1401/1, 14100 Praha 4, Czech Republic*
[4]*Dipartimento di Matematica e Fisica, Università degli Studi Roma Tre, Via della Vasca Navale 84, I-00146 Roma, Italy*
[5]*University de Strasbourg, CNRS, Observatoire Astronomique de Strasbourg, UMR 7550, F-67000 Strasbourg, France*
[6]*Space Science Data Center, Agenzia Spaziale Italiana, Via del Politecnico snc, I-00133 Roma, Italy*
[7]*INAF Osservatorio Astronomico di Roma, Via Frascati 33, I-00078 Monte Porzio Catone (RM), Italy*
[8]*MIT Kavli Institute for Astrophysics and Space Research, Massachusetts Institute of Technology, 77 Massachusetts Avenue, Cambridge, MA 02139, USA*
[9]*Istituto Nazionale di Fisica Nucleare, Sezione di Pisa, Largo B. Pontecorvo 3, I-56127 Pisa, Italy*
[10]*Dipartimento di Fisica, Università di Pisa, Largo B. Pontecorvo 3, I-56127 Pisa, Italy*
[11]*Physics Department and McDonnell Center for the Space Sciences, Washington University in St. Louis, St. Louis, MO 63130, USA*

Downloaded from https://academic.oup.com/mnras/article/516/4/5907/6731657 by INIST-CNRS INEE INSB user on 06 July 2023

[12]*School of Mathematics, Statistics, and Physics, Newcastle University, Newcastle upon Tyne NE1 7RU, UK*
[13]*Department of Physics and Kavli Institute for Particle Astrophysics and Cosmology, Stanford University, Stanford, CA 94305, USA*
[14]*Université Grenoble Alpes, CNRS, IPAG, F-38000 Grenoble, France*
[15]*Astronomical Institute, Charles University, V Holesovickach 2, CZ-18000 Prague, Czech Republic*
[16]*Dipartimento di Fisica, Università degli Studi di Roma 'Tor Vergata', Via della Ricerca Scientifica 1, I-00133 Roma, Italy*
[17]*Istituto Nazionale di Fisica Nucleare, Sezione di Roma 'Tor Vergata', Via della Ricerca Scientifica 1, I-00133 Roma, Italy*
[18]*Department of Astronomy, University of Maryland, College Park, MD 20742, USA*
[19]*Department of Physics and Astronomy, FI-20014 University of Turku, Finland*
[20]*Nordita, KTH Royal Institute of Technology and Stockholm University, Hannes Alfvéns väg 12, SE-10691 Stockholm, Sweden*
[21]*Space Research Institute of the Russian Academy of Sciences, Profsoyuznaya Str. 84/32, Moscow 117997, Russia*
[22]*National Astronomical Observatories, Chinese Academy of Sciences, 20A Datun Road, Beijing 100101, China*
[23]*Instituto de Astrofísica de Andalucía-CSIC, Glorieta de la Astronomía s/n, E-18008 Granada, Spain*
[24]*INAF Osservatorio Astronomico di Cagliari, Via della Scienza 5, I-09047 Selargius (CA), Italy*
[25]*NASA Marshall Space Flight Center, Huntsville, AL 35812, USA*
[26]*Istituto Nazionale di Fisica Nucleare, Sezione di Torino, Via Pietro Giuria 1, I-10125 Torino, Italy*
[27]*Dipartimento di Fisica, Università degli Studi di Torino, Via Pietro Giuria 1, I-10125 Torino, Italy*
[28]*INAF Osservatorio Astrofisico di Arcetri, Largo Enrico Fermi 5, I-50125 Firenze, Italy*
[29]*Dipartimento di Fisica e Astronomia, Università degli Studi di Firenze, Via Sansone 1, I-50019 Sesto Fiorentino (FI), Italy*
[30]*Istituto Nazionale di Fisica Nucleare, Sezione di Firenze, Via Sansone 1, I-50019 Sesto Fiorentino (FI), Italy*
[31]*Institut für Astronomie und Astrophysik, Universität Tübingen, Sand 1, D-72076 Tübingen, Germany*
[32]*RIKEN Cluster for Pioneering Research, 2-1 Hirosawa, Wako, Saitama 351-0198, Japan*
[33]*California Institute of Technology, Pasadena, CA 91125, USA*
[34]*Yamagata University, 1-4-12 Kojirakawa-machi, Yamagata-shi 990-8560, Japan*
[35]*Osaka University, 1-1 Yamadaoka, Suita, Osaka 565-0871, Japan*
[36]*University of British Columbia, Vancouver, BC V6T 1Z4, Canada*
[37]*Department of Physics, Faculty of Science and Engineering, Chuo University, 1-13-27 Kasuga, Bunkyo-ku, Tokyo 112-8551, Japan*
[38]*Institute for Astrophysical Research, Boston University, 725 Commonwealth Avenue, Boston, MA 02215, USA*
[39]*Department of Astrophysics, St. Petersburg State University, Universitetsky pr. 28, Petrodvoretz, 198504 St. Petersburg, Russia*
[40]*Finnish Centre for Astronomy with ESO, 20014 University of Turku, Finland*
[41]*Graduate School of Science, Division of Particle and Astrophysical Science, Nagoya University, Furo-cho, Chikusa-ku, Nagoya, Aichi 464-8602, Japan*
[42]*Hiroshima Astrophysical Science Center, Hiroshima University, 1-3-1 Kagamiyama, Higashi-Hiroshima, Hiroshima 739-8526, Japan*
[43]*Department of Physics, The University of Hong Kong, Pokfulam, C694+RP Ma Liu Shui, Hong Kong*
[44]*Department of Astronomy and Astrophysics, Pennsylvania State University, University Park, PA 16802, USA*
[45]*Center for Astrophysics | Harvard & Smithsonian, 60 Garden St, Cambridge, MA 02138, USA*
[46]*INAF Osservatorio Astronomico di Brera, Via E. Bianchi 46, I-23807 Merate (LC), Italy*
[47]*Dipartimento di Fisica e Astronomia, Università degli Studi di Padova, Via Marzolo 8, I-35131 Padova, Italy*
[48]*Mullard Space Science Laboratory, University College London, Holmbury St Mary, Dorking, Surrey RH5 6NT, UK*
[49]*Anton Pannekoek Institute for Astronomy & GRAPPA, University of Amsterdam, Science Park 904, NL-1098 XH Amsterdam, the Netherlands*
[50]*Guangxi Key Laboratory for Relativistic Astrophysics, School of Physical Science and Technology, Guangxi University, Nanning 530004, China*

This paper has been typeset from a TEX/LATEX file prepared by the author.

Downloaded from https://academic.oup.com/mnras/article/516/4/5907/6731657 by INIST-CNRS INEE INSB user on 06 July 2023